CrossMark

Tip of the Red Giant Branch Distances with JWST: An Absolute Calibration in NGC 4258 and First Applications to Type Ia Supernova Hosts

Gagandeep S. Anand[1] , Adam G. Riess[1,2] , Wenlong Yuan[2] , Rachael Beaton[1,2] , Stefano Casertano[1], Siyang Li[2] , Dmitry I. Makarov[3], Lidia N. Makarova[3] , R. Brent Tully[4] , Richard I. Anderson[5] , Louise Breuval[2] , Andrew Dolphin[6,7] , Igor D. Karachentsev[3], Lucas M. Macri[8] , and Daniel Scolnic[9]

[1] Space Telescope Science Institute, 3700 San Martin Drive, Baltimore, MD 21218, USA
[2] Department of Physics and Astronomy, Johns Hopkins University, Baltimore, MD 21218, USA
[3] Special Astrophysical Observatory of the Russian Academy of Sciences, Nizhnij Arkhyz, Karachay-Cherkessia 369167, Russia
[4] Institute for Astronomy, University of Hawaii, 2680 Woodlawn Drive, Honolulu, HI 96822, USA
[5] Institute of Physics, École Polytechnique Fédérale de Lausanne (EPFL), Observatoire de Sauverny, 1290 Versoix, Switzerland
[6] Raytheon, 1151 E. Hermans Road, Tucson, AZ 85756, USA
[7] University of Arizona, Steward Observatory, 933 North Cherry Avenue, Tucson, AZ 85721, USA
[8] NSF's NOIRLab, 950 N Cherry Avenue, Tucson, AZ 85719, USA
[9] Department of Physics, Duke University, Durham, NC 27708, USA

Abstract

The tip of the red giant branch (TRGB) allows for the measurement of precise and accurate distances to nearby galaxies based on the brightest ascent of low-mass red giant branch stars before they undergo the helium flash. With the advent of JWST, there is great promise to utilize the technique to measure galaxy distances out to at least 50 Mpc, significantly further than the Hubble Space Telescope's (HST's) reach of 20 Mpc. However, with any standard candle, it is first necessary to provide an absolute reference. Here, we use Cycle 1 data to provide an absolute calibration in the F090W filter. F090W is most similar to the F814W filter commonly used for TRGB measurements with HST, which had been adopted by the community due to its minimal dependence on the underlying metallicities and ages of stars. The imaging we use was taken in the outskirts of NGC 4258, which has a direct geometrical distance measurement from the Keplerian motion of its water megamaser. Utilizing several measurement techniques, we find $M_{\mathrm{TRGB}}^{\mathrm{F090W}} = -4.362 \pm 0.033$ (stat) ± 0.045 (sys) mag (Vega) for the metal-poor TRGB. We also perform measurements of the TRGB in two Type Ia supernova hosts, NGC 1559 and NGC 5584. We find good agreement between our TRGB distances and previous determinations of distances to these galaxies from Cepheids ($\Delta = 0.01 \pm 0.06$ mag), with these differences being too small to explain the Hubble tension ($\sim$0.17 mag). In addition, we showcase the serendipitous discovery of a faint dwarf galaxy near NGC 5584.

1. Introduction

The tip of the red giant branch (TRGB) has become an increasingly prolific way to measure precise and accurate distances to nearby galaxies (Lee et al. 1993; Karachentsev et al. 2006; Rizzi et al. 2007; Jang & Lee 2015; McQuinn et al. 2017; Beaton et al. 2019; Durbin et al. 2020; Anand et al. 2021a; Shen et al. 2021). With the Advanced Camera for Surveys (ACS) instrument presently operating on board the Hubble Space Telescope (HST), measurements of galaxy distances accurate to 5% can be performed out to 10 Mpc with a single orbit of time. Indeed, TRGB distances to ∼500 galaxies have been obtained and uniformly analyzed under the umbrella of the Extragalactic Distance Database's (Tully et al. 2009) Color–Magnitude Diagrams and Tip of the Red Giant Branch Distances Catalog[10] (Jacobs et al. 2009; Anand et al. 2021b).

The underlying premise for its use as a standard candle is relatively straightforward—stars continue to fuse hydrogen into

helium within a shell around their inert helium cores as they ascend the red giant branch (RGB). For low-mass stars ($0.5 < M < 2 M_{\odot}$), once the helium core reaches a critical mass and temperature, the conditions become suitable for ignition of helium fusion within the core, and the star rapidly rearranges its structure and becomes a much fainter horizontal branch star. Importantly, the luminosity at the TRGB is essentially independent of the initial stellar mass of the low-mass precursor, allowing us to exploit it as a standard candle. In practice, complications come from (1) the effects of line blanketing, (2) varying populations of asymptotic giant branch (AGB) stars right near and above the TRGB, and (3) the presence of dust and crowding within the host galaxy, among others. These issues can be greatly reduced, if not eliminated, by (1) performing measurements in filters where the magnitude of the TRGB has little to no variation with underlying metallicity over a broad range of observed colors, and (2) performing measurements in the uncrowded outer regions of galaxies or alternatively, carefully correcting for crowding via artificial star experiments). More detailed discussions of the use of the TRGB as a standard candle can be found in the literature (e.g., Serenelli et al. 2017; Beaton et al. 2018).

With the advent of JWST (Gardner et al. 2023; Rigby et al. 2023) and its NIRCam imager (Rieke et al. 2023), there is great promise to extend the reach of the TRGB out to much

---

[10] Available for public access at edd.ifa.hawaii.edu.

Table 1
Observation Log for the Data Used in This Paper

Date	Epoch	Exposure	SW Filter	Exp. time (s)
2023-01-30	N5584–Epoch 1	009001_03101_*	F090W	418.7 × 4
2023-01-30	N5584–Epoch 1	009001_05101_*	F150W	526.1 × 4
2023-02-21	N5584–Epoch 2	010001_02101_*	F090W	418.7 × 4
2023-02-21	N5584–Epoch 2	010001_02103_*	F150W	526.1 × 4
2023-05-02	N4258–Epoch 1	005001_03101_*	F090W	257.7 × 4
2023-05-02	N4258–Epoch 1	005001_03103_*	F150W	365.1 × 4
2023-05-17	N4258–Epoch 2	006001_03101_*	F090W	257.7 × 4
2023-05-17	N4258–Epoch 2	006001_03103_*	F150W	365.1 × 4
2023-06-30	N1559–Epoch 1	001001_02101_*	F090W	418.7 × 4
2023-06-30	N1559–Epoch 1	001001_04101_*	F150W	526.1 × 4
2023-07-15	N1559–Epoch 2	002001_03101_*	F090W	418.7 × 4
2023-07-15	N1559–Epoch 2	002001_03103_*	F150W	526.1 × 4

Note. All data was rerun with the `jwst_1130.pmap` or greater context version. The name of all observations starts with "jw01685".

further distances due to its greater sensitivity, sharper resolution, and the increased intrinsic brightness of red giants in the near-infrared. Indeed, a look at the Early Release Science observations of the Wolf–Lundmark–Mellote galaxy (Weisz et al. 2023) shows that JWST/NIRCam is capable of reaching down to at least $m_{F090W} = 30$ mag, allowing TRGB measurements out to at least 50 Mpc (while allowing for photometry that reaches 1 mag below the TRGB).

As we will show, even relatively modest exposure times can allow for substantially further measurements of the TRGB than can be done with equivalent exposure times on HST (even after accounting for the increased JWST overheads). To allow for measurements of galaxy distances via the TRGB with JWST observations, we present an initial *absolute* calibration of the F090W TRGB magnitude with Cycle 1 data taken in the megamaser host galaxy NGC 4258. We also highlight the effectiveness of F090W for JWST TRGB measurements by showcasing applications to two Type Ia supernova (SN Ia) host galaxies (NGC 1559 and NGC 5584) that lie at ∼20 Mpc.

2. Data

The data used in this paper was obtained via the Cycle 1 JWST proposal GO-1685 (Riess et al. 2021). The main objective of this program is to obtain precise photometry of Cepheid variables, Mira variables, and RGB stars, with the goal of reducing systematics along the distance ladder, and as a result, the measurements of the Hubble constant. One of the galaxies targeted with this program was NGC 4258, which is host to a water megamaser that allows for the determination of a highly precise geometric distance to this galaxy (Humphreys et al. 2013; Reid et al. 2019). The data was taken in two separate visits, with the F090W, F150W, and F277W filters, although we do not use the long-wavelength (F277W) images in this paper (see the discussion in Section 3). We have reprocessed all the underlying data to the `jwst_1130.pmap` or greater context files,[11] which include recent updates to the NIRCam flat fields introduced in `jwst_1125.pmap`, as well as to the zero-points introduced in `jwst_1126.pmap`. We note that our photometry is performed using the Vega-Vega zero-points, and not the Sirius-Vega zero-points.[12] Notably, the

---

[11] See a full description of updates at jwst-crds.stsci.edu.
[12] See the explanations provided at https://jwst-docs.stsci.edu/jwst-near-infrared-camera/nircam-performance/nircam-absolute-flux-calibration-and-zero-points.
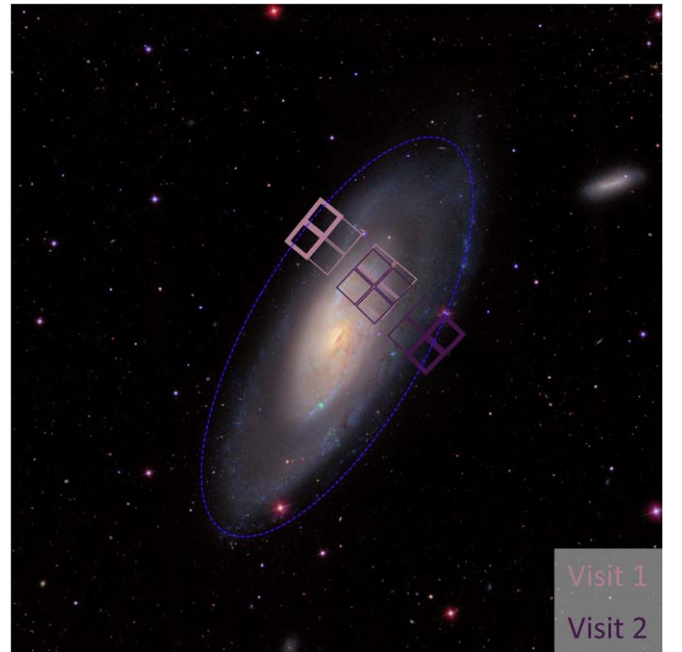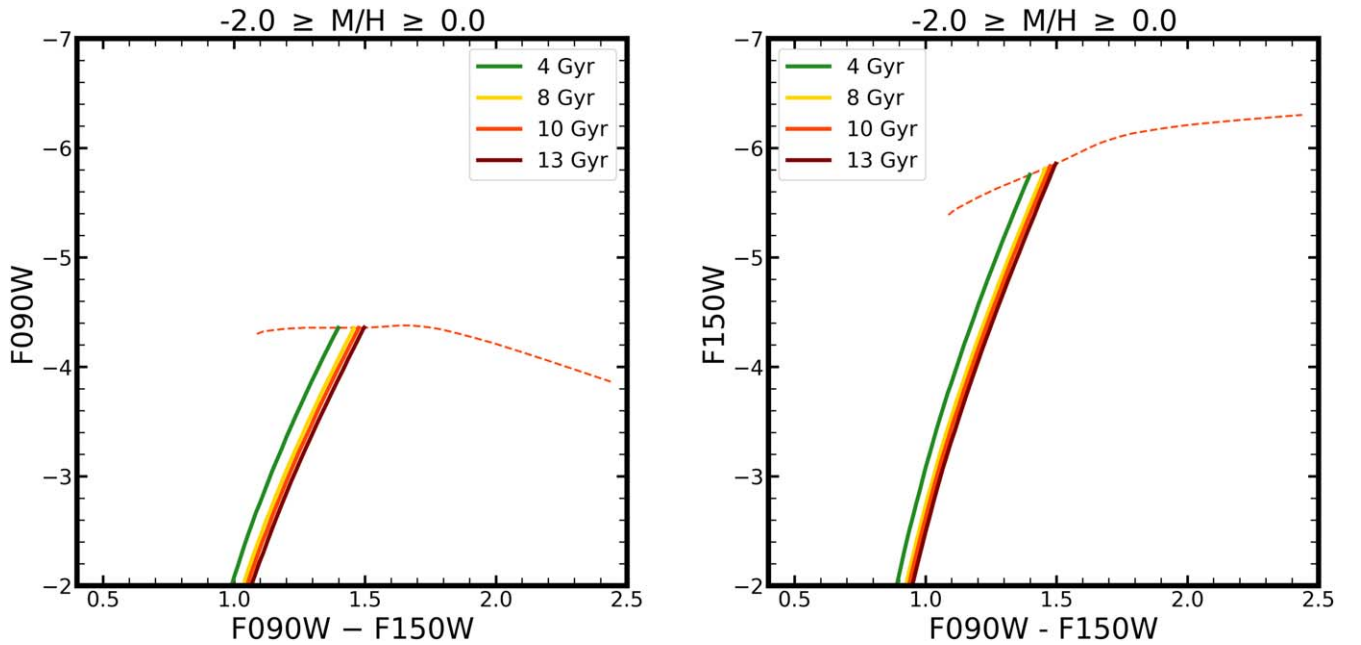

Figure 1. An SDSS (Alam et al. 2015) *gri* color composite of NGC 4258, where north is up and east is to the left. Overlaid on the SDSS imaging are the footprints of the two visits of our observations in NGC 4258 covered by JWST GO-1685. The dashed blue line indicates D_{25}, or the 25th *B*-band magnitude isophote from de Vaucouleurs et al. (1991)—only stars external to this radius are used for our baseline TRGB measurements. All stars found within the outermost chips from each visit (in bold) were used for our spatial selection variant (see Table 2).

uncertainties in the flux calibrations with this latest suite of updates are "now less than 1% for most filter/detector combinations", including those used with our program. Table 1 contains additional details about the individual observations, and Figure 1 shows footprints of our NGC 4258 JWST observations overlaid on SDSS *gri* imaging (Alam et al. 2015).

The inclusion of F090W imaging in our program allows us to measure the TRGB in a filter where there is little to no expected variation of the TRGB over a modest range of colors (the metallicity and age variations are projected onto the color). This is very similar to the case with HST's F814W filter (see Figure 1 in Freedman et al. 2020), which has been by far the most popular filter with which to perform HST TRGB measurements (Jacobs et al. 2009; Anand et al. 2021b). The

Figure 2. PARSEC RGB isochrones in our choice of JWST filters (Bressan et al. 2012). The solid lines show populations of varying underlying ages, and the dashed orange line shows the predicted variation of the absolute magnitude of the TRGB as a function of metallicity ($-2.0 \geqslant M \geqslant 0.0$ dex) for the 10 Gyr population. In F090W, there is minuscule variation with age over the range of 4–13 Gyr (< 0.005 mag), and still little variation with metallicity (< 0.02 mag) over the color range of F090W–F150W = 1.15–1.75 mag. The situation in F150W is much different, where the absolute magnitude of the TRGB is a sharp function of age and metallicity.

inclusion of the secondary filter F150W allows us to generate a color–magnitude diagram (CMD) and prevent contamination by young stellar populations (e.g., main-sequence stars and supergiants). Figure 2 shows PARSEC (Bressan et al. 2012) RGB isochrones in our choice of JWST filters for a range of stellar ages (solid lines). It can be appreciated that the anticipated brightness of the TRGB in F090W has effectively zero (< 0.005 mag) dependence on stellar age for sufficiently old ($\geqslant 4$ Gyr) stellar populations, which to our knowledge of galaxy formation and evolution populate essentially every nearby galaxy.[13] Also shown is the dependence of the F090W magnitude of the TRGB on the underlying stellar metallicity (for a 10 Gyr stellar population, in the dashed line). There is great constancy up until F090W–F150W $\sim$1.8 mag, after which the TRGB begins to tilt downward. In particular, between F090W and F150W = 1.15–1.75, there is only $\sim$0.02 mag of variation in the absolute magnitude of the TRGB in F090W. The same plot is repeated on the right-hand side of Figure 2, except with F150W as the y-axis. It can be seen that while the absolute magnitude of the TRGB is substantially brighter, there is also a large variation with both metallicity and age. While the precise details (such as the predicted absolute magnitude) differ among different families of isochrones (e.g., BaSTI; Pietrinferni et al. 2004, MIST; Choi et al. 2016), the overall picture is the same—F090W is an incredibly stable place to measure the TRGB.

Our chosen filter set is in contrast to another Cycle 1 program (Freedman et al. 2021) that aims, in part, to measure TRGB distances to nearby SN Ia host galaxies with F115W as the primary filter. With F115W, there is substantial variation over even small ranges of colors in the observed magnitude of the TRGB (about half as much as seen with F150W in

Figure 2). While this slope may be *rectified* before making the measurement (Madore et al. 2009, 2018), such a process increases the uncertainty in the underlying measurements. And though there is some benefit due to the increased brightness of the TRGB in F115W when compared with F090W, the main benefit of reduced exposure times may not be worth the increased uncertainties, especially in cases where the highest fidelity TRGB measurements are desired (e.g., for the eventual purposes of measuring the Hubble constant). Additionally, for more nearby galaxies (within $\sim$20 Mpc), JWST visit times are largely overhead dominated, and filter choice makes a relatively small difference in the total charged times. Indeed, a Cycle 2 program (Tully et al. 2023) that aims to connect the TRGB and SBF distance scales (as an alternative to the traditional Cepheid and SNe Ia route) is set to use the same filter set as the data from GO-1685. We note that the JWST Early Release Science (ERS) Program for Resolved Stellar Populations (Weisz et al. 2023) utilizes both of our chosen filters, indicating there is strong community support for their use for general resolved stellar populations science.

3. Data Reduction

We perform point-spread function (PSF) photometry on the underlying stage 2 images (*cal.fits), with the stage 3 F150W image (*i2d.fits) as the reference frame used for source detection and mutual image alignment. We treat the photometry for each visit independently, except for NGC 5584 (which has overlapping visits in its halo, and greatly benefits from the doubled exposure time). Our choice of software for PSF photometry is DOLPHOT (Dolphin 2000, 2016), along with its NIRCam module (Weisz et al. 2023; D. R. Weisz et al. 2024, in preparation). Specifically, we use the latest major release version of DOLPHOT and its NIRCam PSFs, which are from 2023 April 6. We note that there have been two minor

---

[13] There are less than a handful of *candidate* young galaxies in the local Universe, including the Peekaboo dwarf galaxy (Karachentsev et al. 2023).
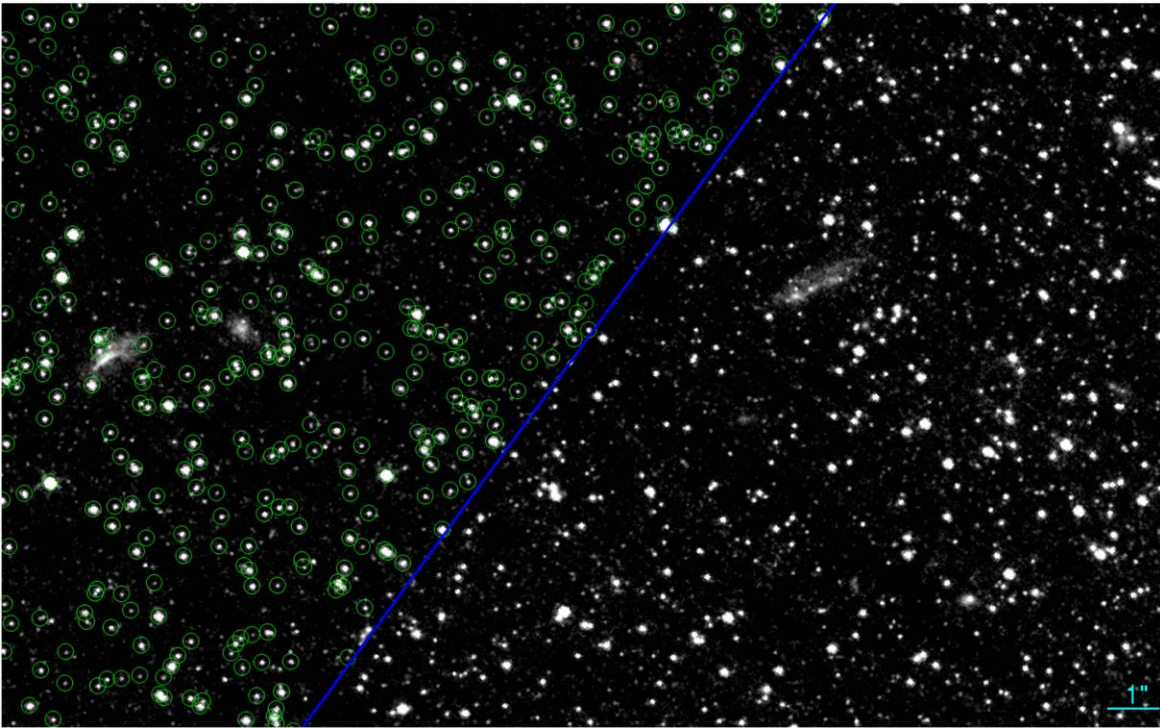
Figure 3. A $22'' \times 14''$ cutout from our F150W reference frame image of Visit 1 shown with an arcsinch stretch. The green circles represent stellar detections that pass our quality criteria and a radial selection exterior to D_{25} (shown in blue). A $1''$ cyan bar is shown for scale in the bottom right. It can be appreciated that the stars in the final list are well resolved and are located in a relatively uncrowded portion of the outer regions of NGC 4258.

updates since then. The first was on 2023 October 11, and this update only changed the default zero-points to the Sirius-Vega system. However, we retain the usage of the original Vega-Vega magnitude system. A second update was provided on 2023 December 2, which provided the "−etctime" option for adjusting the exposure times in the image headers to be in line with the exposure time calculator (ETC) values. As we will discuss shortly, changes brought upon by the use of this option are not particularly relevant for the very high signal-to-noise ratio (S/N) data to be presented for NGC 4258.

We follow the recommendations for reduction parameters outlined in the DOLPHOT NIRCam manual.[14] We note that the pixel scale of the long-wavelength channel ($0''.063$) is much coarser than that of the short-wavelength channel ($0''.031$), resulting in data that is of noticeably worse quality. Combined with the fact that there are currently minor but nonzero photometric impacts by running simultaneous short-wavelength and long-wavelength photometry,[15] we opt to analyze only the short-wavelength NIRCam data in this work.

A great deal of the initial output photometry from DOLPHOT contains detections of low quality. To cull our initial photometry and generate a high-quality source list, we adopt a modified version of the quality cuts given by Warfield et al. ([2023]), which were developed using the ERS data from Weisz et al. ([2023]). Specifically, we select sources with (1) crowding < 0.5; (2) sharpness^2 $\leqslant 0.01$; (3) object type $\leqslant 2$; (4) S/N $\geqslant 5$; and (5) error flag $\leqslant 2$. The quality cuts are applied to both filters (F090W and F150W), except for object type, which

is not filter-specific. An image cutout from the first visit with the stellar detections overlaid can be seen in Figure 3 (after applying the spatial cut described in Section 4.1). We provide our DOLPHOT photometry on GitHub.[16]

To quantify the levels of completeness, photometric error, and bias present in our data, we perform artificial star experiments within DOLPHOT. One at a time, we insert and recover ∼100,000 stars of varying ranges of input magnitudes and colors for each chip and record these results. The artificial stars are processed with the same quality cuts as those applied to the genuine stellar photometry.

An important note, of which we became aware of toward the end of writing this manuscript, is that there are discrepancies between the JWST exposure times provided within the image headers when compared with those provided by the JWST ETC (the former can be over 10% longer in some instances). This mismatch leads to some ambiguity in the determination of the true photometric uncertainties determined via both Poisson noise characteristics and artificial star experiments, especially in parts of the CMD with low S/N. However, we note that the NGC 4258 data is of exceptionally high S/N near the magnitude of the TRGB, where these concerns should have a negligible overall impact. As shown in Figure 4, the photometric completeness curve remains near 100% over 1 mag *below* the TRGB. Similarly, photometric bias is not a concern until we reach much fainter magnitudes. The same may or may not be said for our SN host galaxies, for which the TRGB appears at much fainter magnitudes (see Section 6 for more details). For this reason, we only present edge detection measurements of the TRGB for our SN hosts, and reserve a

---

[14] http://americano.dolphinsim.com/dolphot/dolphotNIRCam.pdf
[15] At present, these can be greatly reduced, but not entirely eliminated with the use of the "warmstart" option—see Riess et al. ([2023b]) for a lengthier discussion.

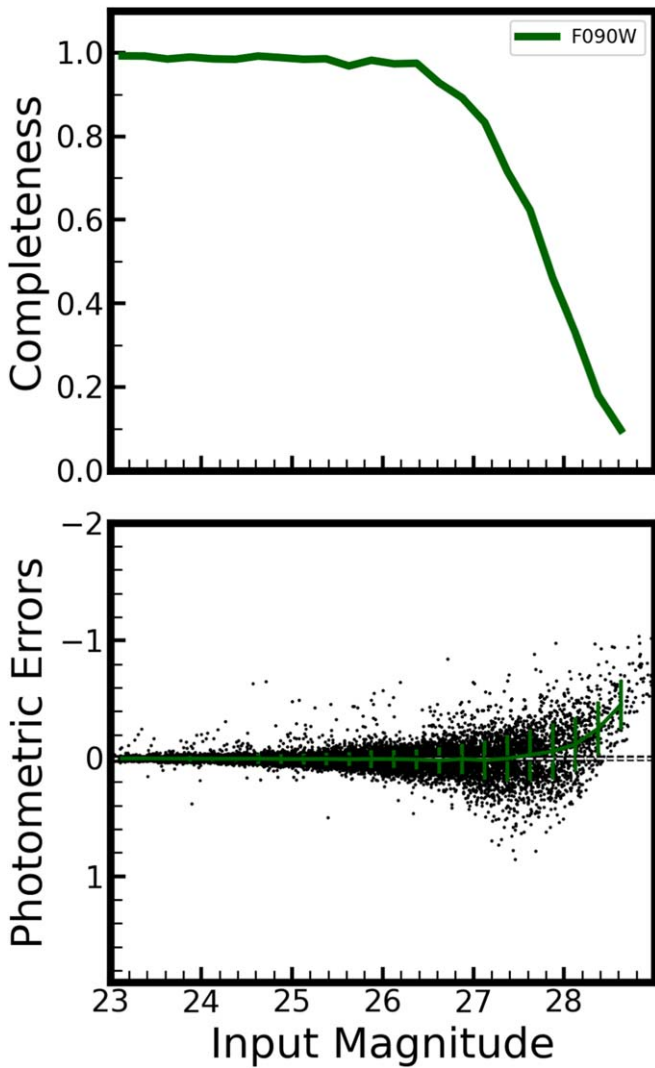[16] https://github.com/gsanand/anand24_jwst_trgb

Figure 4. Results from F090W artificial star experiments for NGC 4258 used for our baseline TRGB results (though only two out of four methods utilize the artificial stars). The top panel shows the completeness curve, which measures the percentage of injected stars that were successfully recovered (including meeting all of our quality criteria). The bottom panel shows the offset between injected and recovered stars (black points), as well as the overall photometric bias (green line). The key point here is that the effects of photometric completeness and bias are entirely negligible near the magnitude of the TRGB ($m_{\mathrm{F090W}} \sim 25.0$ mag). Note that the TRGB measurement tools described later do not use the simple binned versions of these curves shown here, but instead smoothed versions to avoid errors from their apparent jaggedness.

more detailed analysis, including methods that rely on artificial star results, to a later paper.

4. Analysis

Broadly speaking, two distinct methods have been used in the literature to measure the TRGB. The first set involves using an edge detection algorithm (typically a Sobel filter) to locate the discontinuity that is to be expected with the onset of the TRGB (Lee et al. 1993; Sakai et al. 1999; Mager et al. 2008; Jang et al. 2018). This is a conceptually simple technique, though there are differences between applications, such as the bin width used to construct the luminosity function and whether or not the luminosity function is smoothed before applying an edge detector (and if so, how). The second methodology involves fitting a model luminosity function to

the data. This approach was introduced by Méndez et al. (2002), where they adopt a theoretical luminosity function of the general form[17]

$$\psi = \begin{cases} 10^{a(m-m_{\mathrm{TRGB}})+b}, & m - m_{\mathrm{TRGB}} \geqslant 0 \\ 10^{c(m-m_{\mathrm{TRGB}})}, & m - m_{\mathrm{TRGB}} < 0 \end{cases} \quad (1)$$

where a is the power-law slope for stars below the TRGB, c is the power-law slope for stars above the TRGB, and b is the strength of the discontinuity. Further enhancements presented in Makarov et al. (2006) introduce the ability to incorporate results from artificial star experiments, which allows one to account for photometric bias, completeness, and errors present in the data. Wu et al. (2014) present a modified version using a nonlinear least-squares method based on a Levenberg–Marquardt algorithm instead of the Broyden–Fletcher–Gold-farb–Shanno (BFGS) maximum likelihood algorithm used by Makarov et al. (2006).

In this work, we compare results from several iterations of both of the above methods using the same underlying photometry. This will highlight any differences introduced by adopting distinct measurement techniques.

4.1. Spatial Selections

Figure 1 shows that the majority of our JWST observations lie within the disk of NGC 4258 (intentionally, as to measure Cepheid variables). Many previous works have discussed the importance of limiting TRGB measurements to the regions of galaxies that are relatively uncrowded and unaffected by dust internal to the host galaxy (Makarov et al. 2006; Anand et al. 2018; Beaton et al. 2019; Hoyt et al. 2021). For NGC 4258 specifically, Jang et al. (2021) adopt a radial selection of stars outside a semimajor axis cut of $14''$, in part guided by a relatively high-sensitivity H I map from Heald et al. (2011). However, we note that such high-sensitivity H I data is not available for many nearby galaxies (including many SN Ia hosts), and thus presents difficulties when trying to adopt similar spatial cuts for TRGB measurements in other galaxies.

In this work, we adopt the same, simple radial selection as Anand et al. (2022), namely, the 25th B-magnitude isophote from de Vaucouleurs et al. (1991) (D_{25}) as shown by the dashed blue line in Figure 1. We find 23,268 sources that pass our quality cuts outside this region (for reference, there are ~100,000 sources within an individual NIRCam SW chip for observations centered on the disk of NGC 4258). We note that isophotal radii are simpler to measure from existing all-sky ground-based surveys and can provide a more uniform method of spatial selections (as they account for differing sizes of galaxies).

Another potential avenue of performing spatial cuts relies on selection regions with relatively low numbers of young, main-sequence stars in their CMDs (Anand et al. 2021b; Li et al. 2023; Scolnic et al. 2023; Wu et al. 2023). We note that the radial cut we adopt for this work results in a relatively low ratio of main-sequence/giant branch stars. Specifically, blue stars (crudely defined as those with F090W–F150W <0.5 mag, based on the appearance of the main-sequence stars in the CMD) make up less than one out of every 28 stars within a magnitude range of 0.5 mag above and below the TRGB,

---

[17] The definitions of a, b, and c differ between Méndez et al. (2002) and Makarov et al. (2006), and we choose to adopt the definitions from the latter.
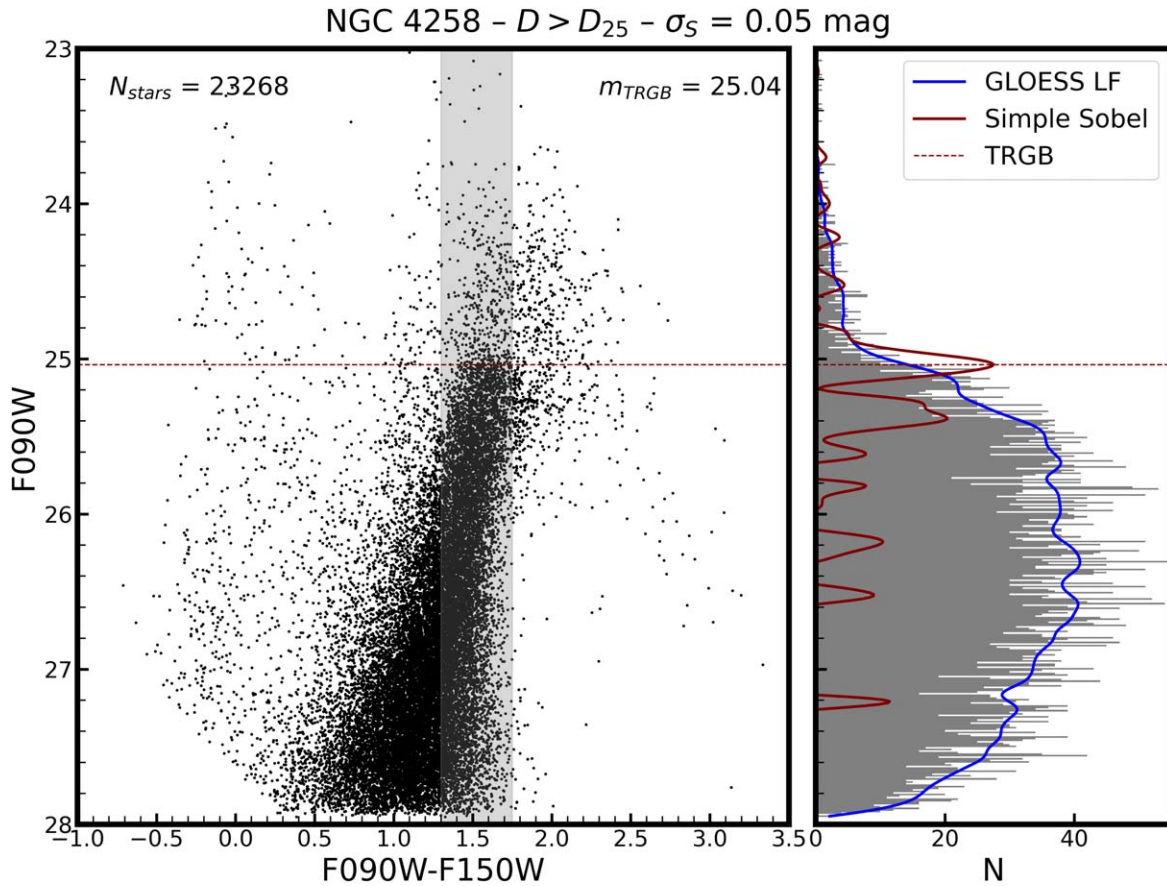
Figure 5. Our baseline edge detection result for the TRGB measurement in NGC 4258. The left panel shows the underlying CMD from our spatially trimmed region, and the gray band shows our limited color selection region. In the right-hand panel, the binned (gray) and GLOESS smoothed (blue) luminosity functions are visible, as well as the output from the Sobel filter (maroon). The data near the TRGB is of exceptionally high quality, as it is nearly 3 mag brighter than the faint limit of $S/N = 5$.

indicating there is minimal contamination from young stellar populations. Regardless, to further reduce the level of contamination from young stellar populations, we will adopt a color selection to the CMD before performing our TRGB measurements. Additionally, we will also present results based on just the outermost two of eight chips from each visit (effectively a crude spatial cut) to test our sensitivity to the adopted spatial criterion.

Lastly, we ensure that the artificial stars undergo the same set of spatial selections, so as not to create a mismatch between the environments in which the selected genuine stars and artificial stars reside.

4.2. Color Selections

Earlier, we mentioned that there is only $\sim$0.02 mag of anticipated variation in the absolute magnitude of the TRGB in F090W between colors of F090W–F150W = 1.15–1.75 mag. This would provide a natural color selection for which to limit our TRGB analysis with. However, we find that even with our adopted spatial selection, there is a small population of what we believe are supergiants, lying along the blue end of this color band. To prevent the influence of these young stars on our measurements, we further restrict our color selection to within F090W–F150W = 1.30–1.75 mag. That being said, we will later show that the precise color selection makes little difference to our measurements.

4.3. Edge Detection Results

The first group of measurement techniques involves edge detection. To construct the underlying luminosity function, we first bin the photometry with a small bin width ($\sigma_{\mathrm{bin}} = 0.01$ mag), using only the stars in our limited color range. Before applying the edge detector, we smooth the underlying luminosity function with a Gaussian locally weighted regression smoothing (GLOESS) algorithm (Persson et al. 2004; Hatt et al. 2017) to reduce the underlying noise present due to stochastic and/or star formation history driven variations in the underlying stellar populations. Given that our CMD extends $\sim$3 mag below the TRGB and that our CMD is relatively well populated even within our selected color band ($\sim$3200 stars in the first magnitude below the measured TRGB), we adopt a relatively small baseline smoothing scale of $\sigma_S = 0.05$ mag.

To perform the edge detection, we employ the use of a Sobel filter with a kernel of $[-1, 0, 1]$, which is effectively a discrete first derivative. Our baseline result is shown in Figure 5, from which we measure $m_{\mathrm{TRGB}} = 25.04 \pm 0.02$ mag, where the uncertainty is determined via 1000 bootstrap resampling with replacement trials, where each time the TRGB is remeasured (similar to Cohen et al. 2018; Hoyt 2023). To test for any variations with the adopted value of σ_S, we run through a range of smoothing scales from 0.04–0.15 mag (see Figure 6), which bracket the values that are generally used in the literature. From $\sigma_S = 0.04$–0.12 mag, we find no change in the measurement of m_{TRGB}. However, with smoothing scales higher than $\sigma_S = 0.12$
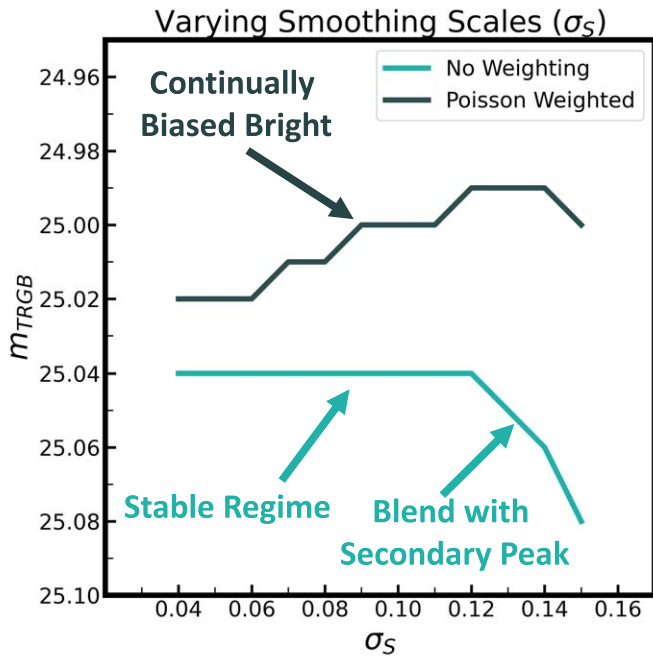
Figure 6. The variation of $m_{\rm TRGB}$ as a function of the underlying smoothing scale (σ_S), for both the unweighted and the Poisson-weighted Sobel edge detectors. The unweighted case shows a stable response until a relatively large smoothing scale, where the TRGB response begins to blend with a fainter edge response. The Poisson-weighted response shows a general trend of becoming brighter with increased smoothing scales, with no readily apparent cause.

mag, we find that the peak in the edge detection response identified as the TRGB begins to blend with a second set of peaks near $m_{\rm F090W} \sim 25.3$ mag, causing the measurement to become skewed faintward due to a modest jump in the underlying luminosity function.

We note that our baseline result does not employ the use of further weighting to the edge detection output, as done by some previous works (Hatt et al. 2017; Freedman et al. 2019; Hoyt 2023). We test the use of a Poisson weighting scheme over the same range of smoothing scales tested for the unweighted edge detection. It can be seen in Figure 6 that the weighted edge detection results start becoming brighter with $\sigma_S > 0.06$ mag. This matches the behavior seen from simulated luminosity functions as well as the observed Large Magellanic Cloud red giant luminosity function (Anderson et al. 2023). Unlike the case with the unweighted edge detection, there is no significant peak brightward of the one that is identified as the TRGB. Instead, we suspect this may be an inherent feature of weighted edge detectors, and thus avoid utilizing them further. We recommend that future studies should closely examine the potential systematic effects of adopting different smoothing scales in their work, especially when employing a further weighting algorithm.

To test the effects of applying a cruder spatial selection, we also perform our measurement on the combined CMD generated from the outermost two of eight SW NIRCam chips from each visit (the bold chips in Figure 1). We measure nearly the same value of $m_{\rm TRGB} = 25.05 \pm 0.02$ mag, indicating that our results are not highly sensitive to the precise spatial selection that is adopted. Indeed, Jang et al. (2021) found that their measured TRGB values in NGC 4258 did not significantly vary over a broad range of radial cuts (from $6'' > {\rm SMA} > 22''$ in their mosaic). Subdividing the crude spatial cuts further into their individual visits results in $m_{\rm TRGB} = 25.06 \pm 0.05$ mag for

Visit 1 (east), and $m_{\rm TRGB} = 25.04 \pm 0.02$ mag for Visit 2 (west). Again, our general point stands, in that our results are quite resilient to the precise spatial cut applied.

Additionally, we note that while we exercise additional care in our color selection (mainly to eliminate the contamination from a small sample of yellow supergiants), a much broader color range gives a very similar result—that is, increasing the color range to 0.5–2.5 mag results in $m_{\rm TRGB} = 25.05 \pm 0.02$ mag, which is only 0.01 mag offset from our baseline result. This difference is likely very small due to the fact that we do not have a large sample of higher metallicity TRGB stars in the outskirts of NGC 4258. These stars would appear faintward of the low-metallicity TRGB, and could otherwise skew our result toward substantially fainter magnitudes.

4.4. Fitting a Model Luminosity Function

Next, we turn to the model fitting solutions to determine the value of $m_{\rm TRGB}$. We will explore the use of three different tools. First, using the original maximum likelihood TRGBTOOL described in Makarov et al. (2006), we find a value of $m_{\rm TRGB} = 25.07 \pm 0.02$ mag. We also use the modified TRGBTOOL presented in Wu et al. (2014). As mentioned earlier, the underlying fitting algorithm in this work (a Levenberg–Marquardt nonlinear least-squares algorithm) differs from one utilized by Makarov et al. (2006), a BFGS maximum likelihood algorithm. Notably, the tool described by Wu et al. (2014) requires binning of the underlying luminosity function. The only change we make to the procedure described in Wu et al. (2014) is that we lower the bin width from 0.05 to 0.02 mag, an option we are afforded due to the relatively well-populated CMDs. With this version of the tool, we find $m_{\rm TRGB} = 25.07 \pm 0.01$ mag, where the error is determined from the square root of the variance of the TRGB magnitude. We also find that varying the bin width between 0.01 and 0.05 mag in steps of 0.01 mag varies the measured TRGB magnitude by less than 0.005 mag. For illustration, we show the baseline model fit to the observed luminosity function using the (Wu et al. 2014) methodology in Figure 7.

Finally, we also use a maximum likelihood algorithm-based tool that does not employ artificial stars. This method searches for the set of parameters in the broken power-law luminosity function model that maximizes the likelihood of the sample, given the model and model parameters (the same underlying principle as Méndez et al. 2002). A two-dimensional version of this tool is described in Li et al. (2022), where the extra dimension is required due to the need to jointly model individual red giants in the Milky Way that are not located at the same line-of-sight distance. We use a one-dimensional version here, and find $m_{\rm TRGB} = 25.04 \pm 0.01$ mag, where the error is determined from the inverse Hessian matrix.

As with the edge detection results, we also perform a series of the above three fits, but using a cruder spatial cut which involves just examining the outer two chips from each of the two visits. With the original TRGBTOOL (Makarov et al. 2006), we find $m_{\rm TRGB} = 25.09 \pm 0.01$ mag. With the tool described in Wu et al. (2014), we find $m_{\rm TRGB} = 25.06 \pm 0.01$ mag. Lastly, with a one-dimensional version of the maximum likelihood tool from Li et al. (2022; in which a two-dimensional version is required as Milky Way stars are not all at the same distance), we find $m_{\rm TRGB} = 25.05 \pm 0.01$ mag. The scattering of these results from their original values with the cruder spatial cut is cause for close examination of the adopted spatial selection
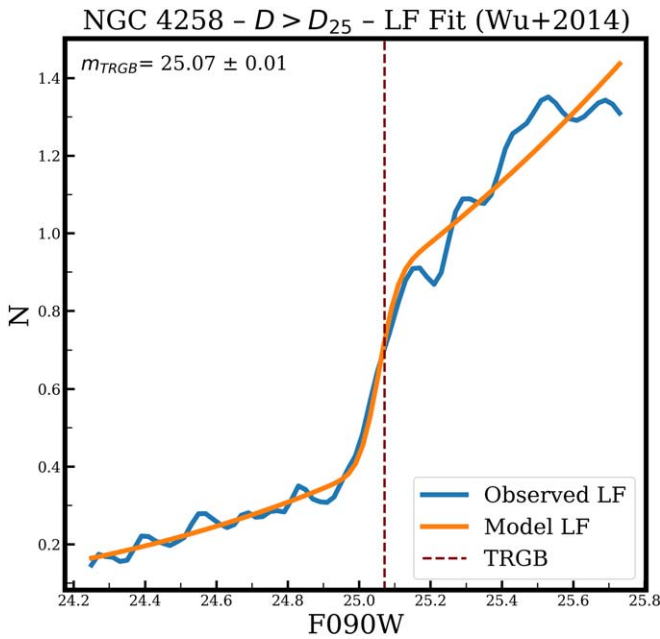
Figure 7. The baseline model fit for the TRGB measurement via the method of Wu et al. (2014), from which we find $m_{\rm TRGB} = 25.07 \pm 0.01$ mag.

criteria with future TRGB measurements. Although the differences are modest in our case (0.01–0.02 mag), these changes may be noticeably larger with data that is either lower S/N or taken in different regions of the host galaxy.

Lastly, we also test the effects of adopting a broader color baseline with our luminosity function fitting techniques. We increase the color baseline from F090W–F150W = 1.30–1.75 mag to 0.5–2.5 mag. For the original TRGBTOOL (Makarov et al. 2006), we now find $m_{\rm TRGB} = 25.07 \pm 0.02$ mag, which is identical to the version with the stricter color selection (but with a larger uncertainty). With the modified TRGBTOOL (Wu et al. 2014), we find $m_{\rm TRGB} = 25.06 \pm 0.01$ mag, or 0.01 brighter than the baseline result with this methodology. Lastly, with the one-dimensional version of the Li et al. (2022) tool, we find $m_{\rm TRGB} = 25.05 \pm 0.01$ mag, or 0.01 mag fainter than the baseline result.

The modest (0.01–0.02 mag) differences we see with a much broader color selection for the luminosity function fitting techniques are likely reflective of the fact that we simply do not have many high-metallicity RGB stars in our spatially trimmed region. If working with a data set with a substantial portion of high-metallicity RGB stars near the tip, we anticipate our results would be skewed toward a fainter magnitude. This situation is similar to the same tests with a Sobel filter, where again we did not see a substantial difference when broadening the color range.

4.5. Differences among Measurement Routines

We provide a summary of all of our measurement techniques and their resultant TRGB magnitudes in Table 2. The table includes the four baseline results for each distinct measurement methodology and two variants for each (one that varies the color selection and a second that varies the spatial selection).

It is interesting to note that the baseline results could be grouped into two categories, with one being brighter (25.04 mag) than the other (25.07 mag). However, the split is not upon the edge detection versus luminosity function fitting

methodologies, but instead on whether or not artificial stars are included in the analysis. We speculate that this difference of 0.03 mag could arise from the fact that the photometric error of stars near the tip is 0.04 mag in F090W (see Figure 4), similar to the level offset seen between the results (whereas the photometric bias is <0.01 mag). It is possible that the techniques that do not rely on artificial stars are triggering off a set of up-scattered TRGB stars (whereas those that do use artificial stars take this effect into account in their modeling of the luminosity functions). This effect could explain offsets between TRGB measurements by different groups of the same galaxies in the literature (Jang et al. 2021; Anand et al. 2022). On the other hand, this could be reading too much into our results, and the differences may just arise from underlying uncertainties in the various fitting procedures, which may underreport the true uncertainties. Yet another alternative is that the artificial star procedures need further refinement, with the minor NIRCam exposure time issues (see Section 3 for a brief discussion) coming into play. Future, more detailed investigations are warranted.

Broadly speaking, methodological differences in TRGB measurements for the same underlying data at the level of ~0.04 mag are common in the literature on a case-by-case basis (Anand et al. 2022). Avoiding a systematic uncertainty between measurements at this level is difficult without substantial effort to match photometric reduction techniques, noise properties, populations via selection, TRGB measurement techniques, etc. While an error at this level is less relevant for a common galaxy, it is most significant in the case of NGC 4258, which serves as a calibrator of many.

5. Absolute Calibration

To provide our absolute calibration of the TRGB in F090W, we begin with our value of $m_{\rm TRGB} = 25.055 \pm 0.02$ mag, where the measurement is the simple average of our four baseline techniques and the uncertainty is the larger of the reported values (two methods provide 0.01 mag, and two provide 0.02 mag). To proceed further, we must first determine the amount of foreground extinction caused by the Milky Way. We used the Fitzpatrick (1999) reddening law with $R_V = 3.1$, convolved with the transmission functions of the Johnson B, Johnson V, F090W, and F150W filters, to determine the effective reddening relationships between these filters. This analysis yielded reddening coefficients of $A_{\rm F090W}/E(B - V) = 1.4156$ and $A_{\rm F150W}/E(B - V) = 0.6021$. Thus, from $E(B - V) = 0.014$ (Schlafly & Finkbeiner 2011), we determine $A_{\rm F090W} = 0.0198$ mag and $A_{\rm F150W} = 0.0084$ mag. Correcting our measured value for foreground extinction, we find $m_{\rm TRGB}^{\rm F090W,0} = 25.035$ mag. The value for the geometrical distance modulus to NGC 4258 provided by Reid et al. (2019) is $\mu = 29.397 \pm 0.032$ mag, or $D = 7.576 \pm 0.082$ (stat.) ± 0.076 (sys.) Mpc. Subtracting the two distance moduli, we find $M_{\rm TRGB}^{\rm F090W} = -4.362$ mag.

Now, onto the important matter of the uncertainty associated with our calibration. We lay out the separate sources of uncertainty in Table 3, as done similarly in Table 5 in Jang et al. (2021). The individual uncertainties are separated by whether or not they could be reduced with additional observations around NGC 4258 (i.e., statistical versus systematic). For instance, the initial TRGB measurement is assigned a statistical uncertainty of 0.02 mag (as mentioned at the beginning of this subsection), and an additional systematic

Table 2
Summary of Our Four Baseline TRGB Measurements, Followed by Two Variants for Each (Adjusting the Spatial Selection and Color Ranges)

Methodology	Color Range	Spatial Selection	m_{TRGB} (mag)	$\pm$ (mag)	Method Reference
Simple Sobel	1.30–1.75	$D > D_{25}$	25.04	0.02	e.g., Freedman et al. (2019) w/o weighting
LF fitting	1.30–1.75	$D > D_{25}$	25.07	0.02	e.g., Makarov et al. (2006)
LF fitting	1.30–1.75	$D > D_{25}$	25.07	0.01	e.g., Wu et al. (2014)
LF fitting (w/o art. stars)	1.30–1.75	$D > D_{25}$	25.04	0.01	e.g., Li et al. (2022)
Simple Sobel	1.30–1.75	Outer chips	25.05	0.02	e.g., Freedman et al. (2019) w/o weighting
LF fitting	1.30–1.75	Outer chips	25.09	0.01	e.g., Makarov et al. (2006)
LF fitting	1.30–1.75	Outer chips	25.06	0.01	e.g., Wu et al. (2014)
LF fitting (w/o art. stars)	1.30–1.75	Outer chips	25.05	0.01	e.g., Li et al. (2022)
Simple Sobel	0.50–2.50	$D > D_{25}$	25.05	0.02	e.g., Freedman et al. (2019) w/o weighting
LF fitting	0.50–2.50	$D > D_{25}$	25.07	0.02	e.g., Makarov et al. (2006)
LF fitting	0.50–2.50	$D > D_{25}$	25.06	0.01	e.g., Wu et al. (2014)
LF fitting (w/o art. stars)	0.50–2.50	$D > D_{25}$	25.05	0.01	e.g., Li et al. (2022)

Table 3
Uncertainty Budget for Our Absolute Calibration of $M_{\mathrm{TRGB}}^{\mathrm{F090W}}$

Uncertainty	Result (mag)	σ_{stat} (mag)	σ_{sys} (mag)
TRGB measurement	25.055	0.02	0.02
Intrinsic TRGB variation	⋯	⋯	0.02
Color selection	⋯	0.01	⋯
Spatial selection	⋯	0.01	⋯
WebbPSF model	⋯	0.02	⋯
NIRCam PSF stability	⋯	0.01	⋯
NIRCam zero-points	⋯	⋯	0.02*
DOLPHOT photometry	⋯	⋯	0.03*
$m_{\mathrm{TRGB}}^{\mathrm{F090W}}$	25.055	0.033	0.028
A_{F090W}	0.0198	⋯	0.014
$m_{\mathrm{TRGB}}^{\mathrm{F090W,0}}$	25.035	⋯	⋯
Maser distance modulus	29.397	⋯	0.032
$M_{\mathrm{TRGB}}^{\mathrm{F090W}}$	−4.362	0.033	0.045

Note. For the foreground extinction, we assign a conservative systematic uncertainty of 0.014 mag, which is the quadrature sum of one-half of the measured extinction and an additional 0.01 mag of uncertainty due to potential extinction within the outer regions of the host galaxy itself. *The uncertainty terms assigned to the NIRCam zero-points and DOLPHOT photometry will cancel when comparing photometry that uses the same set of NIRCam zero-points and reduction setup, so we do not include these uncertainties in our totals.

uncertainty of 0.02 mag (derived from the spread in our four baseline measurements). A further 0.02 mag systematic contribution is assigned due to the potential variations of $M_{\mathrm{TRGB}}^{\mathrm{F090W}}$ with age and metallicity, which are small but nonzero (see Figure 2). This uncertainty term may also encompass some of the differences seen in recent field-to-field measurements done by the CATs team (Wu et al. 2023), though our TRGB measurement techniques differ from theirs, complicating a more direct comparison. Our color and spatial selections are assigned uncertainties of 0.01 mag each, based on the impact of varying these quantities (shown in Table 2).

Moving to uncertainties resulting from our photometry, we note the presence of small mismatches between the WebbPSF models (Perrin et al. 2014) currently used within DOLPHOT and the observed PSFs, which range between 0% and 2% in the central pixel of the PSF (in either positive and negative

directions, depending upon the particular frame in question). While the PSF models are empirically varied by DOLPHOT on a frame-by-frame basis, we still choose to include a 0.02 mag uncertainty term here. Another small contribution is derived from the stability of the NIRCam PSF, which Riess et al. (2023b) show to be very consistent for the observations in question. One sometimes overlooked uncertainty contribution is the difference between a given photometry setup (e.g., DOLPHOT's NIRCam module with recommended parameters) versus other reductions for which our absolute calibration may be applied to (e.g., with different DOLPHOT setup parameters, or using other photometry packages). We adopt a 0.03 mag uncertainty term here, based on the extensive tests carried out in Jang et al. (2021) and Jang (2023).

Lastly, for the foreground extinction, we assign a conservative systematic uncertainty of 0.014 mag, which is the quadrature sum of one-half of the measured extinction and an additional 0.01 mag of uncertainty due to potential extinction within the outer regions of the host galaxy itself (as also done by Jang et al. 2021). In the end, we find

$$M_{\mathrm{TRGB}}^{\mathrm{F090W}} = -4.362 \pm 0.033\,(\mathrm{stat}) \pm 0.045\,(\mathrm{sys})\,\mathrm{mag}$$

when excluding the error contributions that cancel with comparisons to photometry taken with the same set of NIRCam zero-points, and reduced in an identical manner with DOLPHOT. If these terms are included, the systematic uncertainty increases from 0.045 to 0.058 mag.

We note that while we provide one averaged calibration for our four underlying methods, this can be further tailored to match a particular TRGB measurement methodology. For instance, if one were using the precise methodology outlined in Makarov et al. (2006), a value of $M_{\mathrm{TRGB}}^{\mathrm{F090W}} = -4.347$ mag may be more appropriate. Similarly, $M_{\mathrm{TRGB}}^{\mathrm{F090W}} = -4.377$ mag may be appropriate for providing the absolute calibration to an unweighted Sobel measurement (as we use for NGC 1559 and NGC 5584 in the next section).

6. Application to SN Ia Hosts

With an initial calibration in place, we are able to determine absolute distances to other galaxies observed with JWST in the F090W+F150W filter set. Here, we will highlight the cases of NGC 1559 and NGC 5584, which are host to the Type Ia
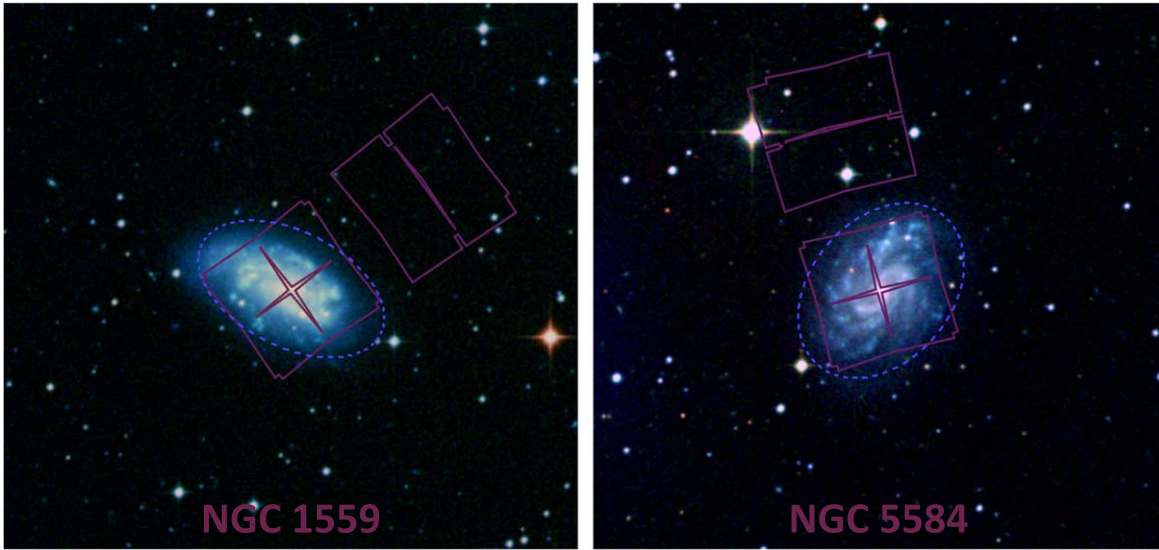
Figure 8. Footprints for our NGC 1559 and NGC 5584 visits, overlaid on Digitized Sky Survey color images. We use only the outer *halo* modules for our TRGB analysis, as they are well removed from the spiral disks and lie outside D_{25} (shown as the dashed blue lines).

supernovae (SNe Ia) SN2005df (Evans & Gilmore 2005) and SN2007af (Nakano & Itagaki 2007), respectively.

6.1. NGC 5584

NGC 5584 was observed as part of the same JWST program as NGC 4258, with the main difference being greater exposure times and field placement. In particular, the outer NIRCam module placements from each visit are mostly overlapping, with a minor orientation difference between the two (see the right-hand side of Figure 8). This decision was made to provide greater depth for TRGB measurements, given that the Cepheid distance to this galaxy is ~23 Mpc (Riess et al. 2022a). As mentioned in Riess et al. (2023b), NGC 5584 is an important galaxy for examining the Hubble tension, as it (1) is near the mean distance of the SH0ES galaxies, (2) contains a plethora of known Cepheids, and (3) on its own, as a singular target of comparison, is nearly 3σ inconsistent with $H_0 \sim 67.5$ km s^{-1} Mpc^{-1} based on results from the Planck satellite (Planck Collaboration et al. 2020).

A TRGB distance to NGC 5584 was first presented by Jang & Lee (2015), who found $\mu = 31.76 \pm 0.04$ (random) ± 0.12 (systematic) mag, which was measured in the outskirts of the spiral disk using HST data acquired to measure Cepheids. A rescaled version of this same TRGB measurement was utilized by Freedman et al. (2019) in determining a value of the Hubble constant from the TRGB (instead of Cepheids). However, a reanalysis of the same underlying images by Anand et al. (2022) was unable to measure the TRGB, due to the shallowness of the resulting photometric catalog. Scolnic et al. (2023) came to the same conclusion, using the same photometric catalog produced by Anand et al. (2022). Now, we perform an analysis of the TRGB from this Cycle 1 JWST data set, which shows a clearly visible presentation of the TRGB. Recently, Riess et al. (2023b) determined a revised Cepheid distance with the B modules (placed on the disk) from this same JWST data set, where they measure a baseline distance modulus of $\mu = 31.813 \pm 0.020$ mag.

We perform the reduction and analysis for NGC 5584 in the same manner as was done with NGC 4258, except that we only use the inner two chips of the A module, which fall within the

target's halo and outside D_{25} (the outer two chips of the A module are too sparsely populated). We also re-extend the left edge of the color baseline to F090W–F150W = 1.15 due to the lack of younger supergiant stars (this alteration impacts the final result by only 0.01 mag). The resulting CMD is shown in Figure 9. We assign the first significant edge detection response to the TRGB, the most common choice in the literature and consistent with the analysis of NGC 4258, or $m_{\mathrm{TRGB}} = 27.47 \pm 0.05$ mag. We note there is a substantial secondary response of ~0.1 mag fainter. This is not entirely surprising, as the data is of a much lower S/N than it is for NGC 4258, and the underlying CMD is of a sparser nature. Very similar secondary responses have been seen in the literature (see the case of NGC 1316 presented in Hatt et al. 2018), and may also be in part due to variations in the underlying star formation history, assemblies of the stellar halos in question, or other factors.

Accounting for $A_{\mathrm{F090W}} = 0.05$ mag (Schlafly & Finkbeiner 2011), and using the TRGB magnitude from the analogous measurement in NGC 4258 (a simple Sobel filter), we determine $\mu = 31.80 \pm 0.08$ mag, in very good agreement with the recently determined JWST Cepheid distance of $\mu = 31.813 \pm 0.020$ mag (Riess et al. 2023b) and the HST Cepheid distance of $\mu = 31.810 \pm 0.047$ mag (Javanmardi et al. 2021).

While the current situation with the JWST exposure times in image headers prevents the determination of highly precise estimates of S/N for individual stars (in the form of photometric errors), we can still use artificial stars to measure the impact of photometric *bias* on our measurements. The increased exposure times and even lower stellar density levels (when compared to NGC 4258) result in a negligible photometric bias (<0.01 mag) at the magnitude of the TRGB, despite it being notably fainter than in NGC 4258. We anticipate a more rigorous analysis of the data from this JWST program (including results from other measurement routines), along with the other SN hosts from this program (NGC 1448, NGC 1559, and NGC 5643) in a planned future work (S. Li et al. 2024, in preparation).
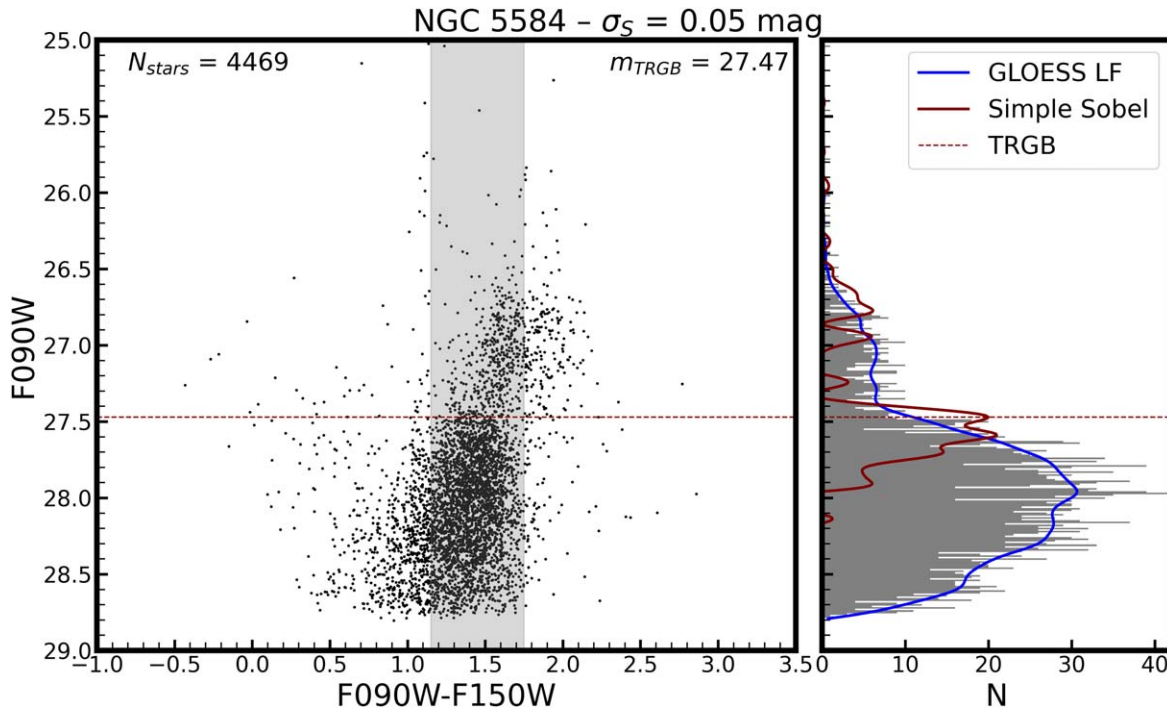
Figure 9. Our simple Sobel TRGB measurement for NGC 5584 was performed in the same manner as our baseline edge detection of NGC 4258 (shown in Figure 5). We use only the outer halo module for our TRGB analysis (see Figure 3 in Riess et al. 2023b), as it is well removed from the spiral disk. The TRGB is clearly visible, even to the eye, with a sharp contrast between the AGB above (which fans off to the right) and the RGB below.

As an entirely distinct point, we note that there is perhaps a visible gap between the brightest RGB stars, and the thermally pulsing-AGB sequence above it (shown as an underdensity of stars in the first couple tenths of a magnitude brighter than the TRGB). This gap is predicted by some stellar models, whereas it is not in others. Here, we simply note the appearance of this potential gap in our data, and highlight that it may be used to calibrate stellar models, as previously suggested by Dalcanton et al. (2012).

6.2. NGC 1559

Along with NGC 5584, we also present a TRGB measurement for NGC 1559. We selected NGC 1559 as a second highlight because it is the only other galaxy from our program without a TRGB measurement in the literature.[18] Additionally, NGC 1559 has an independently determined distance modulus from its Mira variable stars of $\mu = 31.41 \pm 0.05$ (stat.) ± 0.06 (sys.) mag (Huang et al. 2020), which allows for another avenue of comparison.

While we have the same two visit structure for NGC 1559, this galaxy is ~ 0.4 mag closer than NGC 5584, allowing us to securely measure the TRGB from each visit separately. While there is a modest orientation difference between the two visits (see the left-hand side of Figure 8), much of the underlying stellar population is the same, and a second measurement allows for an additional check of internal stability.

We follow the same procedure as described for NGC 5584, including the color baseline of F090W–F150W = 1.15–1.75. For our first visit, we find $m_{\mathrm{TRGB}} = 27.17 \pm 0.04$ mag, and for the second visit, we find $m_{\mathrm{TRGB}} = 27.13 \pm 0.02$ mag. As in NGC 5584 and NGC 4258 we note the presence of a fainter feature,

while in all three cases accepting the brighter. Taking the simple average of these two measurements (and conservatively adopting the larger error), we find $m_{\mathrm{TRGB}} = 27.15 \pm 0.04$ mag (see Figure 10). From Schlafly & Finkbeiner (2011), we determine $A_{\mathrm{F090W}} = 0.04$ mag, and thus we find $\mu = 31.49 \pm 0.07$ mag. This is consistent with both the Cepheid determination of 31.49 ± 0.06 mag (Riess et al. 2022a), and the Mira determination of 31.41 ± 0.08 mag (Huang et al. 2020). As with NGC 5584, the photometric bias is negligible at the magnitude of the TRGB, and we anticipate a more multifaceted and thorough analysis of this data set in a future paper.

6.3. Comparing Cepheid and TRGB Distances

An important issue under study in the context of the current Hubble tension is the level of agreement between values of the Hubble constant derived from SN Ia calibrated through either Cepheids, TRGB, and Mira distances as well as from masers, surface brightness fluctuations (SBFs), and the Tully–Fisher relation, independent of SNe Ia. The Cepheid-SN Ia route gives a result of $H_0 = 73.04 \pm 1.04$ km s^{-1} Mpc^{-1} with the most recent major SH0ES release (Riess et al. 2022a), with more recent updates (Riess et al. 2022b; Murakami et al. 2023) providing a value of 73.29 ± 0.90 km s^{-1} Mpc^{-1}.

A prominent measurement of H_0 was derived via a TRGB calibration of SNe Ia luminosities by the CCHP team (Freedman et al. 2019), who found $H_0 = 69.8 \pm 0.8$ (stat) ± 1.7 (sys) km s^{-1} Mpc^{-1}. Freedman (2021) then provided an updated value of 69.8 ± 0.6 (stat) ± 1.6 (sys) km s^{-1} Mpc^{-1}. An alternate reduction from the same underlying HST data but with different photometric and TRGB measurement methodologies by Anand et al. (2022) resulted in $H_0 = 71.5 \pm 1.5$ km s^{-1} Mpc^{-1}. Another alternate measurement by Scolnic et al. (2023), which uses the same photometry as Anand et al. (2022) from the Extragalactic Distance Database (EDD;

---

[18] Neither does NGC 5468, but at a distance of ~ 40 Mpc, our data set is too shallow to allow for such a measurement.
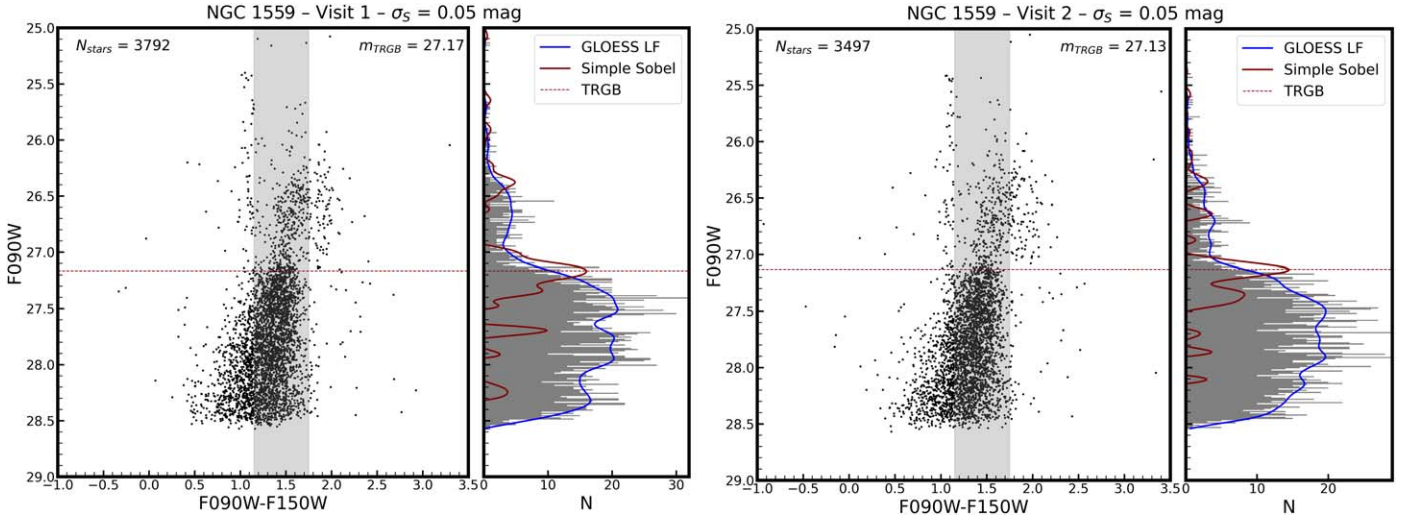
Figure 10. The two pairs of panels show our simple Sobel TRGB measurements for each visit of NGC 1559, performed in the same manner as our baseline edge detection of NGC 4258 (shown in Figure 5). Again, we use only the outer halo module for our TRGB analysis (see Figure 8), as it is well removed from the spiral disk.

Tully et al. 2009; Anand et al. 2021b) but with a different approach to standardizing TRGB measurements, finds a baseline result of $H_0 = 73.22 \pm 2.06 \, \mathrm{km \, s^{-1} \, Mpc^{-1}}$.

As discussed by Scolnic et al. (2023), the largest source of differences between the TRGB and Cepheid results is not due to differences between the use of Cepheids and TRGB to measure the distances to SN Ia host galaxies. Rather, they find in their comparisons of distance ladders that the majority of the disagreement between the H_0 values between these studies comes from differences in their treatment of the SN Ia data in the rung following either Cepheids or TRGB. Specifically, the application of peculiar velocity corrections and photometric standardization of different SN surveys at optical wavelengths contributes to a $\sim$2.0 $\mathrm{km \, s^{-1} \, Mpc^{-1}}$ difference between the CCHP and studies that utilize the Pantheon + SN survey (Brout et al. 2022). A recent study by Uddin et al. (2023) that combines Cepheids, TRGB, SN Ia, and SBF, and includes the application of SN Ia peculiar velocity corrections finds $H_0 = 72.5 \pm 1.5 \, \mathrm{km \, s^{-1} \, Mpc^{-1}}$.

For a direct comparison of TRGB and Cepheid measures as they contribute to the Hubble tension, we can circumvent SNe Ia and geometric distance estimates and directly compare distances to individual SN Ia host galaxies determined with each method calibrated with the same geometric source, as is done in Figures 5 and 6 in Freedman et al. (2019) and Figure 23 in Riess et al. (2022a). Here, we provide an updated version of Figure 23 from Riess et al. (2022a) in our Figure 11, which incorporates our two initial measurements of distance to NGC 1559 and NGC 5584. The difference between the HST Cepheid and JWST TRGB distances when calibrated to the same anchor (NGC 4258) is negligible at 0.01 ± 0.06 mag, similar to the minor differences found between comparisons of HST Cepheids and HST TRGB results from the CCHP and EDD teams. With newly obtained and further upcoming JWST data that is appropriate for both Cepheid and TRGB measurements from GO-1685 (Riess et al. 2021), GO-1995 (Freedman et al. 2021), and GO-2875 (Riess et al. 2023a), we anticipate even more robust comparisons between Cepheids and the TRGB in the near future. Comparisons of distances by different methods provide the ability to disentangle components of the distance ladder without reference to H_0, whose calculation is a composite of many steps. For reference, the

approximate size of the Hubble tension is $5 \log(73/67.5) = 0.17$ mag, a difference that is inconsistent with the comparisons presented here, demonstrating that the middle rung of the distance ladder cannot be solely responsible for the tension.

6.4. Discovery of a New Dwarf Galaxy near NGC 5584

While inspecting the images from the first visit to NGC 5584, we noticed what appeared to be a stellar overdensity on the A3 chip that was well off of the main spiral disk (which was focused on with the B module). We consider this stellar overdensity (see the left-hand side of Figure 12) to be a candidate dwarf galaxy in the vicinity of NGC 5584.

While there are two visits to this galaxy, the orientation of the second visit misses half of the body of the dwarf candidate. Additionally, a significant portion of the remaining stars that are covered in the second visit lie in the glow of a diffraction spike of a very bright foreground star, which would likely lead to degraded photometry. For this reason, we only present data from the first visit for this newly discovered candidate dwarf galaxy, NGC 5584-dw1. The CMD of this dwarf galaxy is shown on the right-hand side of Figure 12, limited to the region within the blue circle. The CMD for the entire chip from that same visit is shown in the background in gray points. We reduce the S/N cut to 3 instead of our baseline value of 5 for both filters, in order to probe further down the RGB. It can be seen that the candidate dwarf's CMD is broadly consistent with the underlying CMD from the halo of NGC 5584, with a somewhat lower mean metallicity. We reserve a more detailed analysis of the properties of this newly discovered dwarf galaxy, along with one more found in the outskirts of NGC 5468, to a future paper.

7. Summary and Future Outlook

We present an initial, absolute calibration of the magnitude of the TRGB in the JWST F090W passband based on data taken in the outer regions of the megamaser host NGC 4258. We find $M_{\mathrm{TRGB}}^{\mathrm{F090W}} = -4.362 \pm 0.033 \, \mathrm{(stat)} \pm 0.045 \, \mathrm{(sys)}$ mag, when considering only the relatively metal-poor stars before the high-metallicity *turnover*. The relative constancy of the TRGB in F090W at lower metallicities (traced by the color of
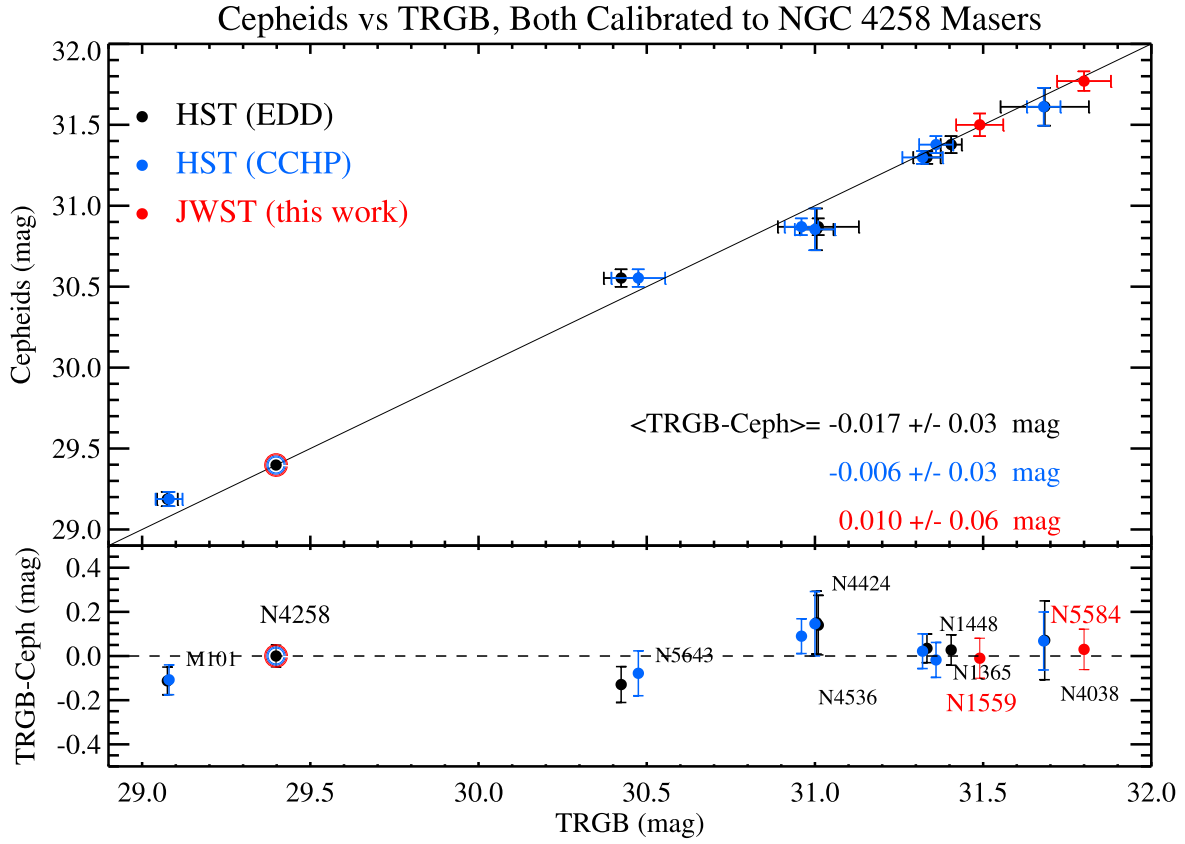
Cepheids vs TRGB, Both Calibrated to NGC 4258 Masers

Figure 11. An updated version of Figure 23 from Riess et al. (2022a), which compares Cepheid and TRGB distances to SN Ia host galaxies. We find excellent agreement between Cepheid and TRGB distances when each set is measured consistently relative to the same anchor (NGC 4258).
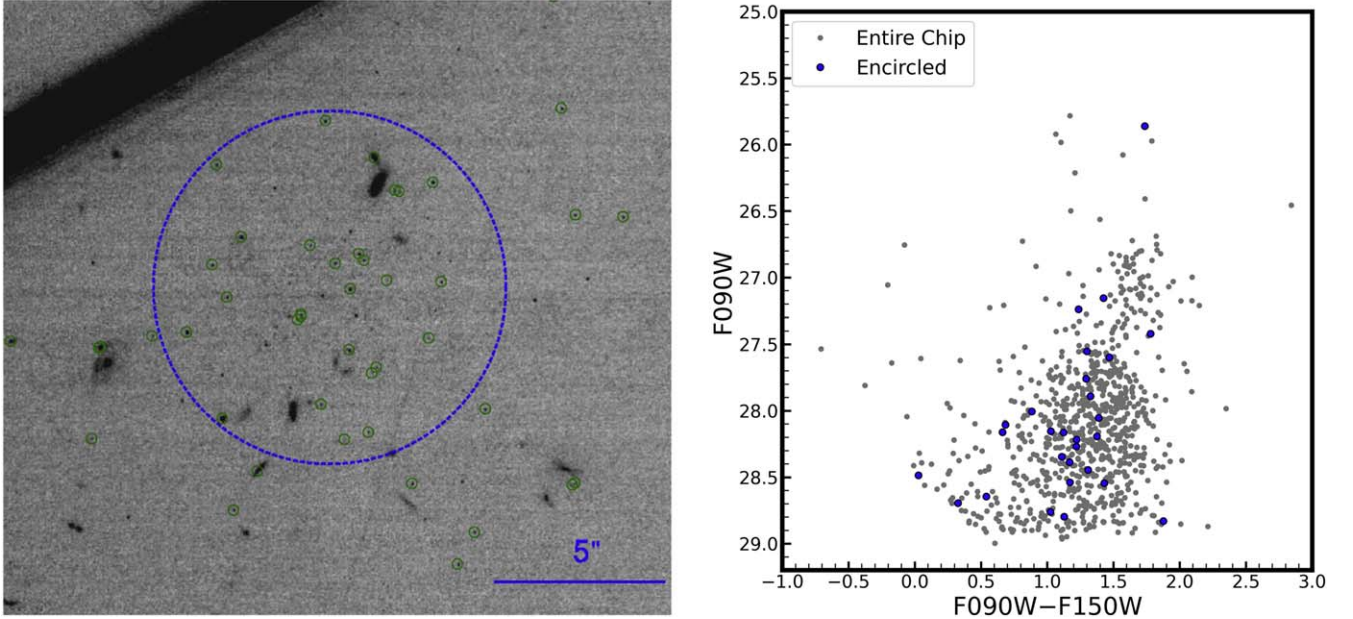

Figure 12. The left-hand panel shows a cutout from the A3 chip of the first visit in NGC 5584. Encircled in blue is a candidate dwarf galaxy (NGC 5584-dw1) we identified upon first inspection of the images, with sources that pass our quality cuts encircled in green. The CMD within the circle is shown on the right in blue points, with the underlying CMD of the rest of the A3 chip shown in gray.

stars) allows it to be used as a standard candle without the need for color *rectification*, as would be required with observations in bluer or redder filters. While we do not present this as a definitive calibration, we believe this work represents a first major step, and that any remaining systematic errors due to

field placement (<0.02 mag) and uncertainties in the underlying photometric calibrations (<0.02 mag) are negligible for most applications (especially as the later would cancel out, when comparing data which uses the same version of NIRCam zero-points).

Our NGC 4258 data, which consists of just 1030 s of exposure time in F090W at each field placement, would allow us to measure distances out to ~19 Mpc (while keeping the TRGB one full magnitude above the S/N = 5 floor). A similar amount of time in F150W would suffice for the TRGB (the F150W data set presented here is somewhat deeper, as it was required for the Cepheid observations). Including overheads, such a visit typically requires less than 2 hr of JWST charged time. This situation represents nearly a factor of 8 increase in volume over a similar setup with HST/ACS (a reach of 10 Mpc with one orbit split between F606W+F814W), highlighting the gains due to JWST's increased sensitivity. While largely not relevant to the measurement of the TRGB within NGC 4258, the increased resolution of NIRCam (compared to ACS/WFC) will be key for measuring TRGB distances out to further distances, where crowding will become an increasingly larger factor. Additionally, K-corrections become relevant for TRGB distances at the 1% level for galaxies $\gtrsim$50 Mpc distant (Anderson 2022).

We also present a preliminary measurement of the TRGB in NGC 1559 and NGC 5584, as a showcase of JWST's capabilities. While the repeatability of the singular HST TRGB measurement in NGC 5584 is a matter of some debate (Jang & Lee 2015; Freedman et al. 2019; Anand et al. 2022), the JWST TRGB measurement is clearly visible, even to the unassisted eye. In the near future, we will use our absolute TRGB calibration to measure well-tested distances to four SN hosts from GO-1685 (NGC 1448, NGC 1559, NGC 5584, NGC 5643), which are host to a total of six SNe Ia. Combined with anticipated TRGB measurements from the upcoming Cycle 2 program GO-2875 (Riess et al. 2023a), an independent appraisal of the Cepheid distance scale (Riess et al. 2022a) is well within reach with just the data already on JWST's schedule.

Our calibration will also be useful as a preliminary absolute calibration of the TRGB + SBF distance scale, where the SBF measurements would take the place of SNe Ia in the final rung of the distance ladder (Cantiello & Blakeslee 2023). In-progress observations from the Cycle 2 JWST Program GO-3055 (Tully et al. 2023) will provide the data needed to determine a secure TRGB calibration for the SBF distance scale. It is incredible to imagine that except for the initial geometric scaling, all other steps of the distance ladder can be obtained with NIRCam, including SBF measurements out into the Hubble flow. This would have the effect of nullifying many mutual sources of error along our proposed Population II distance ladder.

To reiterate, we do not present this as a final calibration of the TRGB in NIRCam's F090W filter. There will be inevitable updates to photometric reference files, zero-points, and flat fields, as well as changes to best practices for PSF photometry with DOLPHOT. Updates to the TRGB calibration presented here from our team will duly follow. What we do present is a well-tested set of measurements in NGC 4258 that form the basis of an initial calibration, which we believe will serve the community well in performing general distance measurements with the TRGB and JWST. Additionally, we are aware of at least one other program (GO-1638; McQuinn et al. 2021) that will present not only a calibration in F090W, but also in a broader range of JWST filters. It is indeed an exciting time for work on the extragalactic distance scale.

ORCID iDs

Gagandeep S. Anand ⓘ https://orcid.org/0000-0002-5259-2314
Adam G. Riess ⓘ https://orcid.org/0000-0002-6124-1196
Wenlong Yuan ⓘ https://orcid.org/0000-0001-9420-6525
Rachael Beaton ⓘ https://orcid.org/0000-0002-1691-8217
Siyang Li ⓘ https://orcid.org/0000-0002-8623-1082
Dmitry I. Makarov ⓘ https://orcid.org/0000-0001-9110-3221
Lidia N. Makarova ⓘ https://orcid.org/0000-0003-0736-7609
R. Brent Tully ⓘ https://orcid.org/0000-0002-9291-1981
Richard I. Anderson ⓘ https://orcid.org/0000-0001-8089-4419
Louise Breuval ⓘ https://orcid.org/0000-0003-3889-7709
Andrew Dolphin ⓘ https://orcid.org/0000-0001-8416-4093
Lucas M. Macri ⓘ https://orcid.org/0000-0002-1775-4859
Daniel Scolnic ⓘ https://orcid.org/0000-0002-4934-5849

References

Alam, S., Albareti, F. D., Allende Prieto, C., et al. 2015, ApJS, 219, 12
Anand, G. S., Lee, J. C., Van Dyk, S. D., et al. 2021a, MNRAS, 501, 3621
Anand, G. S., Rizzi, L., & Tully, R. B. 2018, AJ, 156, 105
Anand, G. S., Rizzi, L., Tully, R. B., et al. 2021b, AJ, 162, 80
Anand, G. S., Tully, R. B., Rizzi, L., Riess, A. G., & Yuan, W. 2022, ApJ, 932, 15
Anderson, R. I. 2022, A&A, 658, A148
Anderson, R. I., Koblischke, N. W., & Eyer, L. 2023, ApJL, 963, L43
Beaton, R. L., Bono, G., Braga, V. F., et al. 2018, SSRv, 214, 113
Beaton, R. L., Seibert, M., Hatt, D., et al. 2019, ApJ, 885, 141
Bressan, A., Marigo, P., Girardi, L., et al. 2012, MNRAS, 427, 127
Brout, D., Taylor, G., Scolnic, D., et al. 2022, ApJ, 938, 111

Cantiello, M., & Blakeslee, J. P. 2023, arXiv:2307.03116
Choi, J., Dotter, A., Conroy, C., et al. 2016, ApJ, 823, 102
Cohen, Y., van Dokkum, P., Danieli, S., et al. 2018, ApJ, 868, 96
Dalcanton, J. J., Williams, B. F., Melbourne, J. L., et al. 2012, ApJS, 198, 6
de Vaucouleurs, G., de Vaucouleurs, A., Corwin, H. G. J., et al. 1991, Third Reference Catalogue of Bright Galaxies (Berlin: Springer)
Dolphin, A. 2016, DOLPHOT: Stellar photometry, Astrophysics Source Code Library, ascl:1608.013
Dolphin, A. E. 2000, PASP, 112, 1383
Durbin, M. J., Beaton, R. L., Dalcanton, J. J., Williams, B. F., & Boyer, M. L. 2020, ApJ, 898, 57
Evans, R., & Gilmore, A. 2005, CBET, 192, 1
Fitzpatrick, E. L. 1999, PASP, 111, 63
Freedman, W. L. 2021, ApJ, 919, 16
Freedman, W. L., Madore, B. F., Hatt, D., et al. 2019, ApJ, 882, 34
Freedman, W. L., Madore, B. F., Hoyt, T., et al. 2020, ApJ, 891, 57
Freedman, W. L., Madore, B. F., Hoyt, T., et al. 2021, Answering the Most Important Problem in Cosmology Today: Is the Tension in the Hubble Constant Real?, JWST Proposal, Cycle 1, ID. #1995, STScI
Gardner, J. P., Mather, J. C., Abbott, R., et al. 2023, PASP, 135, 068001
Hatt, D., Beaton, R. L., Freedman, W. L., et al. 2017, ApJ, 845, 146
Hatt, D., Freedman, W. L., Madore, B. F., et al. 2018, ApJ, 866, 145
Heald, G., Józsa, G., Serra, P., et al. 2011, A&A, 526, A118
Hoyt, T. J. 2023, NatAs, 7, 590
Hoyt, T. J., Beaton, R. L., Freedman, W. L., et al. 2021, ApJ, 915, 34
Huang, C. D., Riess, A. G., Yuan, W., et al. 2020, ApJ, 889, 5
Humphreys, E. M. L., Reid, M. J., Moran, J. M., Greenhill, L. J., & Argon, A. L. 2013, ApJ, 775, 13
Jacobs, B. A., Rizzi, L., Tully, R. B., et al. 2009, AJ, 138, 332
Jang, I. S. 2023, MNRAS, 521, 1532
Jang, I. S., Hatt, D., Beaton, R. L., et al. 2018, ApJ, 852, 60
Jang, I. S., Hoyt, T. J., Beaton, R. L., et al. 2021, ApJ, 906, 125
Jang, I. S., & Lee, M. G. 2015, ApJ, 807, 133
Javanmardi, B., Mérand, A., Kervella, P., et al. 2021, ApJ, 911, 12
Karachentsev, I. D., Dolphin, A., Tully, R. B., et al. 2006, AJ, 131, 1361
Karachentsev, I. D., Makarova, L. N., Koribalski, B. S., et al. 2023, MNRAS, 518, 5893
Lee, M. G., Freedman, W. L., & Madore, B. F. 1993, ApJ, 417, 553
Li, S., Casertano, S., & Riess, A. G. 2022, ApJ, 939, 96
Li, S., Riess, A. G., Scolnic, D., et al. 2023, arXiv:2306.10103
Madore, B. F., Freedman, W. L., Hatt, D., et al. 2018, ApJ, 858, 11
Madore, B. F., Mager, V., & Freedman, W. L. 2009, ApJ, 690, 389
Mager, V. A., Madore, B. F., & Freedman, W. L. 2008, ApJ, 689, 721

Makarov, D., Makarova, L., Rizzi, L., et al. 2006, AJ, 132, 2729
McQuinn, K. B. W., Boyer, M. L., Dolphin, A. E., Newman, M. J. B., & Skillman, E. D. 2021, Securing the TRGB Distance Indicator: A Pre-Requisite for a JWST Measurement of H_0, JWST Proposal, Cycle 1, ID. #1638, STScI
McQuinn, K. B. W., Skillman, E. D., Dolphin, A. E., Berg, D., & Kennicutt, R. 2017, AJ, 154, 51
Méndez, B., Davis, M., Moustakas, J., et al. 2002, AJ, 124, 213
Murakami, Y. S., Riess, A. G., Stahl, B. E., et al. 2023, JCAP, 2023, 046
Nakano, S., & Itagaki, K. 2007, IAU Circ., 8817, 3
Perrin, M. D., Sivaramakrishnan, A., Lajoie, C.-P., et al. 2014, Proc. SPIE, 9143, 91433X
Persson, S. E., Madore, B. F., Krzemiński, W., et al. 2004, AJ, 128, 2239
Pietrinferni, A., Cassisi, S., Salaris, M., & Castelli, F. 2004, ApJ, 612, 168
Planck Collaboration, Aghanim, N., Akrami, Y., et al. 2020, A&A, 641, A6
Reid, M. J., Pesce, D. W., & Riess, A. G. 2019, ApJL, 886, L27
Rieke, M. J., Kelly, D. M., Misselt, K., et al. 2023, PASP, 135, 028001
Riess, A., Anderson, R. I., Breuval, L., et al. 2021, Uncrowding the Cepheids for an Improved Determination of the Hubble Constant, JWST Proposal, Cycle 1, ID. #1685, STScI
Riess, A., Anderson, R. I., Breuval, L., et al. 2023a, Scrutinizing the Dirtiest Cepheids, a Test of the Hubble Tension, JWST Proposal, Cycle 2, ID. #2875, STScI
Riess, A. G., Anand, G. S., Yuan, W., et al. 2023b, ApJL, 956, L18
Riess, A. G., Breuval, L., Yuan, W., et al. 2022b, ApJ, 938, 36
Riess, A. G., Yuan, W., Macri, L. M., et al. 2022a, ApJL, 934, L7
Rigby, J., Perrin, M., McElwain, M., et al. 2023, PASP, 135, 048001
Rizzi, L., Tully, R. B., Makarov, D., et al. 2007, ApJ, 661, 815
Sakai, S., Madore, B. F., & Freedman, W. L. 1999, ApJ, 511, 671
Schlafly, E. F., & Finkbeiner, D. P. 2011, ApJ, 737, 103
Scolnic, D., Riess, A. G., Wu, J., et al. 2023, ApJL, 954, L31
Serenelli, A., Weiss, A., Cassisi, S., Salaris, M., & Pietrinferni, A. 2017, A&A, 606, A33
Shen, Z., Danieli, S., van Dokkum, P., et al. 2021, ApJL, 914, L12
Tully, R. B., Anand, G. S., Blakeslee, J. P., et al. 2023, A TRGB calibration of Surface Brightness Fluctuations, JWST Proposal, Cycle 2, ID. #3055, STScI
Tully, R. B., Rizzi, L., Shaya, E. J., et al. 2009, AJ, 138, 323
Uddin, S. A., Burns, C. R., Phillips, M. M., et al. 2023, arXiv:2308.01875
Warfield, J. T., Richstein, H., Kallivayalil, N., et al. 2023, RNAAS, 7, 23
Weisz, D. R., McQuinn, K. B. W., Savino, A., et al. 2023, ApJS, 268, 15
Wu, J., Scolnic, D., Riess, A. G., et al. 2023, ApJ, 954, 87
Wu, P.-F., Tully, R. B., Rizzi, L., et al. 2014, AJ, 148, 7